**ISSN: 0067-2904**

# Impacts of Heat and Mass Transfer on Magneto Hydrodynamic Peristaltic Flow Having Temperature-dependent Properties in an Inclined Channel Through Porous Media

**Rabiha S. Kareem*, Ahmed M. Abdulhadi**
Department of Mathematics, College of Science, Baghdad University, Baghdad, Iraq

Received: 24/7/ 2019 Accepted: 30/9/2019

**Abstract**

In this paper, we study the impacts of variable viscosity , heat and mass transfer on magneto hydrodynamic (MHD) peristaltic flow in a asymmetric tapered inclined channel with porous medium . The viscosity is considered as a function of temperature. The slip conditions at the walls were taken into consideration. Small Reynolds number and the long wavelength approximations were used to simplify the governing equations. A comparison between the two velocities in cases of slip and no-slip was plotted. It was observed that the behavior of the velocity differed in the two applied models for some parameters. Mathematica software was used to estimate the exact solutions of temperature and concentration profiles. The resolution of the equations to the momentum was based on the perturbation method to find the axial velocity, pressure gradient and trapping phenomenon. The influences of the various flow parameters of the problem on these distributions were debated and proved graphically by figures.

**Key words:** Peristalsis flow, variable viscosity, concentration, heat transfer.

# تاثير انتقال الحرارة والكتلة على التدفق المغناطيسي ذي الخصائص المعتمدة على درجة الحرارة في قناة مائلة من خلال وسط المسامي

**رابحة سليم كريم* ,احمد مولود عبد الهادي**
قسم الرياضيات ، كلية العلوم، جامعة بغداد، بغداد ، العراق

**الخلاصه**

في هذه الورقة ، ناقشنا تأثيرات اللزوجة المتغيرة ، انتقال الحرارة والكتلة على التدفق التمعجي المغنطيسي في قناة مائلة غير متناظرة مدببة مع وجود وسط مسامي. اللزوجة متغيرة حيث تعتمد على درجة الحرارة. تؤخذ شروط الانزلاق في الجدران في الاعتبار. يتم استخدام رقم رينولدز الصغير وتقريب الطول الموجي الطويل لتبسيط المعادلات الحاكمة. وترد مقارنة بين السرعتين في حالة الانزلاق وعدم الانزلاق موضحة في الرسم. لقد لاحظنا أن سلوك السرعة لنموذجين يختلف عن بعضها البعض بالنسبة لبعض المعلمات، تم الحصول على الحل الحقيقي لكل من الحرارة والتركيز بينما استخدمنا طريقة الاضطراب لمعرفة السرعة المحورية،اخيرا ناقشنا تأثير معلمات التدفق المختلفة ويثبت بيانيا من خلال الرسوم.

## 1- Introduction

Nowadays, the peristaltic flow has gained much interest because of its influences in the field of industry and physiology. Peristalsis is a format of fluid transfer caused by a progressive wave of

*Email: rabiha.s77@yahoo.com

region constriction or extension over the length of a flexible channel. In this format, transmission of the fluid occurs in the trend of the wave propagation. The peristalsis flow happens in the human body, as in the movement processes of chyme through digestive tract, urine through the ureter, the swallowed food through the esophagus. and many others [1,2]. This type of flow is extremely expedient in designing several biomedical apparatuses, e.g. the heart - lung device to preserve the blood circulation in dangerous surgeries [3]. This subject was first investigated by Shapiro et al. and Lew et al. [4,5]. The concept of peristaltic transport was subjected to various suppositions, the most well-known among which are the lengthy wavelength and the small Reynolds number.

A non-Newtonian fluid is a fluid whose viscosity is variable based on applied stress or force. It is a fluid whose flow properties are not described by a single constant value of viscosity. It was observed that the physiological fluids with constant viscosity fail to give an accurate grasp when the peristaltic transfer is involved in the lymphatic vessels, small blood vessels and gut. Most studies of peristalsis were applied under constant viscosity. Several recent studies [6-9] investigated the influence of variable viscosity, when the viscosity is dependent on the distance only. However, some researches considered the influence of the viscosity when it is dependent on the temperature [10-12]. Also, It was established that the influences of heat and mass transfer hold significant roles in peristaltic flow, as in blood flux processes, kidney dialysis and cancer medicament. Interesting research attempts investigated the link between the influence of heat and mass transfer on magneto hydrodynamic flows, as studied lately by Zin et al. [13], Gul et al.[14], and Abdellateef et al. [15]. The correlation between the problems of heat and mass transfer through peristaltic flow of MHD fluid on an asymmetric channel was investigated by Kothandapani et al.[16].

The porous medium has a significant role in the analysis of transportation process in industrial mechanisms , bio-fluid mechanics and engineering domains. Several investigators studied the magneto hydrodynamic flow under convective heat and mass transfer through a porous medium. Ramesh and Devakar [17] studied the effects of heat and mass transfer of MHD couple stress fluid with porous medium in a vertical asymmetric channel. Alharbi et al. [18] investigated heat and mass transfer in MHD visco-elastic fluid flux through a porous medium with chemical reaction. Reddy[19] discussed the effect of velocity slip on MHD peristaltic flow in a porous medium with heat and mass transfer.

The aim of the present study is to analyze the MHD fluid with variable viscosity. The related equations were simulated by adopting conservation laws of mass, momentum, energy and concentration. The small Reynolds number and the long wavelength were also executed. The differential equations of the fluid flow were resolved subject to related boundary conditions (slip conditions). A comparative study between the velocity and slip and no-slip conditions was discussed. At the end of the paper, graphical results were shown to display the physical conduct of the various considered parameters.

**2- Formulation The Problem:**

We consider the MHD fluid flow, with variable viscosity in a tapered inclined asymmetric channel with the width of $(d_1 + d_2)$, through a porous medium in two dimensions. The motion is made by sinusoidal wave sequences propagating with constant speed $(c)$ and wavelength on the lengthwise of the channel walls.

The equations of walls geometry are presented as

$$\bar{h}_1(\bar{X},\bar{t}) = d_1 + \bar{m}\bar{X} + a_1 Cos\left[\frac{2\pi}{\lambda}(\bar{X} - c\bar{t})\right] \quad \text{Lower wall} \quad (1)$$

$$\bar{h}_2(\bar{X},\bar{t}) = -d_2 - \bar{m}\bar{X} - a_2 Cos\left[\frac{2\pi}{\lambda}(\bar{X} - c\bar{t}) + \varphi\right] \quad \text{Upper wall} \quad (2)$$

where $(a_1)$ and $(a_2)$ represent the wave amplitudes of the lower and upper walls, respectively, $(\lambda)$ is the wave length , $(c)$ is the velocity of the peristaltic wave , $\bar{t}$ is the time, and $(\bar{m} \ll 1)$ is a non-uniform parameter. $(\bar{X},\bar{Y})$ are the Cartesian coordinates, where $\bar{X}$ is the direction of wave propagation while $\bar{Y}$ is taken normal to it. $(\varphi)$ represents the phase difference with the range $(0 \le \varphi \le \pi)$, in which $(\varphi = 0)$ matches up to the symmetric channel with waves out of phase, while $(\varphi = \pi)$ matches up to the waves in phase, i.e., both channel walls move inward or outward concurrently . Further, $a_1, a_2, d_1, d_2$, and $\varphi$ satisfy the next relation at the inlet of the divergent channel

$$a_1^2 + a_2^2 + 2a_1a_2\, Cos(\varphi) \le (d_1 + d_2)^2 \quad (3)$$

**3- Fundamental Computation of Lorentz Force**

To calculate the Lorentz force, we will apply the magnetic field in the $\overline{\mathrm{Y}}-$ direction and, thereafter, we are interested in the analysis of the impact of magnetic field on the flow. Suppose the fluid to be electrically conducting in the existence of a uniform inclined magnetic field $\vec{B}=(0,\mathrm{B}_0,0)$.

$$\bar{V}\times\bar{B}=\begin{vmatrix}\vec{\imath} & \vec{\jmath} & \vec{k}\\ u & v & 0\\ 0 & B_0 & 0\end{vmatrix}=B_0u\vec{k} \tag{4}$$

Hence

$$\vec{J}=\sigma\left(\vec{V}\times\vec{B}\right)=\sigma B_0u\vec{k} \tag{5}$$

Then, by Ohm's law one has

$$\vec{J}\times\vec{B}=\begin{vmatrix}\vec{\imath} & \vec{\jmath} & \vec{k}\\ 0 & 0 & \sigma B_0u\\ 0 & B_0 & 0\end{vmatrix}=-\sigma B_0^2u\vec{\imath} \tag{6}$$

in which $\vec{J}$ is the current density vector, $(\sigma)$ is the electrical conductivity of fluid, and $(B_0)$ is the magnetic field strength. It is obvious that the influence of magnetic field on the fluid flux is substantial in $\overline{\mathrm{X}}-$ direction .

**4- The Governing Equations**

The governing equations of motion of incompressible MHD fluid model, with variable viscosity, through an inclined tapered asymmetric channel in laboratory frame are

The continuity equation

$$\frac{\partial\bar{U}}{\partial\bar{X}}+\frac{\partial\bar{V}}{\partial\bar{Y}}=0 \tag{7}$$

The momentum equations

$$\rho\left[\frac{\partial\bar{U}}{\partial\bar{t}}+\bar{U}\frac{\partial\bar{U}}{\partial\bar{X}}+\bar{V}\frac{\partial\bar{U}}{\partial\bar{Y}}\right]=-\frac{\partial\bar{P}}{\partial\bar{X}}+2\frac{\partial}{\partial\bar{X}}\left[\bar{\mu}\left(\bar{T}\right)\frac{\partial\bar{U}}{\partial\bar{X}}\right]+\frac{\partial}{\partial\bar{Y}}\left[\bar{\mu}\left(\bar{T}\right)\left(\frac{\partial\bar{V}}{\partial\bar{X}}+\frac{\partial\bar{U}}{\partial\bar{Y}}\right)\right]-\sigma B_0^2\bar{U}+\rho g\alpha_1(\bar{T}-T_0)Sin(\xi)+\rho g\alpha_2(\bar{C}-C_0)Sin(\xi)-\frac{\bar{\mu}\left(\bar{T}\right)}{K_0}\bar{U} \tag{8}$$

$$\rho\left[\frac{\partial\bar{V}}{\partial\bar{t}}+\bar{U}\frac{\partial\bar{V}}{\partial\bar{X}}+\bar{V}\frac{\partial\bar{V}}{\partial\bar{Y}}\right]=-\frac{\partial\bar{P}}{\partial\bar{Y}}+2\frac{\partial}{\partial\bar{Y}}\left[\bar{\mu}\left(\bar{T}\right)\frac{\partial\bar{V}}{\partial\bar{Y}}\right]+\frac{\partial}{\partial\bar{X}}\left[\bar{\mu}\left(\bar{T}\right)\left(\frac{\partial\bar{V}}{\partial\bar{X}}+\frac{\partial\bar{U}}{\partial\bar{Y}}\right)\right]-\frac{\bar{\mu}\left(\bar{T}\right)}{K_0}\bar{V} \tag{9}$$

The energy equation

$$\rho C_p\left[\frac{\partial\bar{T}}{\partial\bar{t}}+\bar{U}\frac{\partial\bar{T}}{\partial\bar{X}}+\bar{V}\frac{\partial\bar{T}}{\partial\bar{Y}}\right]=\kappa\left[\frac{\partial^2\bar{T}}{\partial\bar{X}^2}+\frac{\partial^2\bar{T}}{\partial\bar{Y}^2}\right]+\frac{\partial\bar{q}_r}{\partial\bar{Y}}+Q_0 \tag{10}$$

The concentration equation

$$\frac{\partial\bar{C}}{\partial\bar{t}}+\bar{U}\frac{\partial\bar{C}}{\partial\bar{X}}+\bar{V}\frac{\partial\bar{C}}{\partial\bar{Y}}=D\left[\frac{\partial^2\bar{C}}{\partial\bar{X}^2}+\frac{\partial^2\bar{C}}{\partial\bar{Y}^2}\right]+\frac{DK_T}{T_m}\left[\frac{\partial^2\bar{T}}{\partial\bar{X}^2}+\frac{\partial^2\bar{T}}{\partial\bar{Y}^2}\right] \tag{11}$$

where $\bar{U}$ is the axial velocity, $\overline{\mathrm{V}}$ is the transverse velocity, $\overline{T}$ is the temperature, and $\bar{C}$ is the concentration. $\rho,\ k_0\ ,\bar{P},Q_0,\kappa,B_0,D,\sigma,K_T,T_m,\alpha_1,\alpha_2$ represent the density, permeability parameter , the pressure, constant heat addition/absorption, thermal conductivity, constant magnetic field, coefficient of mass diffusivity, electrical conductivity, thermal diffusion ratio, mean temperature, coefficient of linear thermal expansion, and coefficient of expansion with concentration, respectively.

By Rosseland approximation [20] , the relative heat flux is expressed as

$$\bar{\mathrm{q}}_\mathrm{r}=\frac{4\sigma'}{3\mathrm{k}'}\frac{\partial\mathrm{T}^4}{\partial\overline{\mathrm{Y}}} \tag{12}$$

where $(k')$ and $(\sigma')$ are the mean absorption coefficient and the Stefan- Boltzman constant, respectively. Taking into account that the temperature variance within the fluid mass that flows is adequately small, by Taylor expansion and cancelling higher-order terms, we can write

$$T^4\cong 4T_0^3\bar{T}-3T_0^4 \tag{13}$$

By substituting Eq.(13) into Eq.(12), we get

$$\bar{\mathrm{q}}_\mathrm{r}=-\frac{16\sigma'T_0^3}{3\mathrm{k}'}\frac{\partial\bar{T}}{\partial\bar{Y}} \tag{14}$$

The boundary conditions at the wall are listed below:

Model-1: The appropriate boundary conditions, including wall slip, convective and concentration, are given as follows

$$\bar{U} + \beta_0 \frac{\partial \bar{U}}{\partial \bar{Y}} = 0 \ , \quad \bar{T} = T_1, \quad \bar{C} = C_1 \ at \ \ \bar{Y} = \bar{h}_1 \tag{15}$$

$$\bar{U} - \beta_0 \frac{\partial \bar{U}}{\partial \bar{Y}} = 0 \ , \quad \bar{T} = T_0, \quad \bar{C} = C_0 \ at \ \ \bar{Y} = \bar{h}_2 \tag{16}$$

Model-2: The appropriate boundary conditions, including wall no-slip, convective and concentration , are given as follows

$$\bar{U} = 0 \ , \quad \bar{T} = T_1, \quad \bar{C} = C_1 \ at \ \ \bar{Y} = \bar{h}_1 \tag{17}$$

$$\bar{U} = 0 \ , \quad \bar{T} = T_0, \quad \bar{C} = C_0 \ at \ \ \bar{Y} = \bar{h}_2 \tag{18}$$

The flow phenomenon is fundamentally unsteady in the laboratory coordinate system $(\bar{X}, \bar{Y}, \bar{t})$. However, it can be treated as a steady flow in a coordinate system $(\bar{x}, \bar{y})$, rotating with equal angular velocity as a laboratory coordinate, which moves with the speed of the wave. The relationship between the two frames is described in the following:

$$\bar{y} = \bar{Y}, \ \bar{x} = \bar{X} - c\bar{t} \ , \bar{u} = \bar{U} - c \ , \bar{v} = \bar{V}, \bar{p}(\bar{x}, \bar{y}) = \bar{P}(\bar{X}, \bar{Y}, \bar{T}), \ \ T = \bar{T} \ , \ C = \bar{C} \tag{19}$$

in which $\bar{u}, \bar{v}, \bar{p}, T$ and $C$ designate velocity components, pressure, temperature and concentration in the wave frame, respectively.

After using the conversions in Eq.(19), Eqs.(7)-(11) in the wave frame will be formed as below

$$\frac{\partial(\bar{u}+c)}{\partial(\bar{x}+c\bar{t})} + \frac{\partial \bar{v}}{\partial \bar{y}} = 0 \tag{20}$$

$$\rho\left[\frac{\partial(\bar{u}+c)}{\partial \bar{t}} + (\bar{u}+c)\frac{\partial(\bar{u}+c)}{\partial(\bar{x}+c\bar{t})} + \bar{v}\frac{\partial(\bar{u}+c)}{\partial \bar{y}}\right] = -\frac{\partial \bar{p}}{\partial(\bar{x}+c\bar{t})} + 2\frac{\partial}{\partial(\bar{x}+c\bar{t})}\left[\bar{\mu}\,(T)\frac{\partial(\bar{u}+c)}{\partial(\bar{x}+c\bar{t})}\right] + \frac{\partial}{\partial \bar{y}}\left[\bar{\mu}\,(T)\left(\frac{\partial \bar{v}}{\partial(\bar{x}+c\bar{t})} + \frac{\partial(\bar{u}+c)}{\partial \bar{y}}\right)\right] - \sigma B_0^2(\bar{u}+c) + \rho g \alpha_1 (T - T_0)\sin(\xi) + \rho g \alpha_2 (C - C_0)\sin(\xi) - \frac{\bar{\mu}\,(T)}{K_0}(\bar{u}+c) \tag{21}$$

$$\rho\left[\frac{\partial \bar{v}}{\partial \bar{t}} + (\bar{u}+c)\frac{\partial \bar{v}}{(\bar{x}+c\bar{t})} + \bar{v}\frac{\partial \bar{v}}{\partial \bar{y}}\right] = -\frac{\partial \bar{p}}{\partial \bar{y}} + 2\frac{\partial}{\partial \bar{y}}\left[\bar{\mu}\,(T)\frac{\partial \bar{v}}{\partial(\bar{x}+c\bar{t})}\right] + \frac{\partial}{\partial(\bar{x}+c\bar{t})}\left[\bar{\mu}\,(T)\left(\frac{\partial \bar{v}}{\partial(\bar{x}+c\bar{t})} + \frac{\partial(\bar{u}+c)}{\partial \bar{Y}}\right)\right] - \frac{\bar{\mu}\,(T)}{K_0}\bar{v} \tag{22}$$

$$\rho C_p\left[\frac{\partial T}{\partial \bar{t}} + (\bar{u}+c)\frac{\partial T}{\partial(\bar{x}+c\bar{t})} + \bar{v}\frac{\partial T}{\partial \bar{y}}\right] = \kappa\left[\left(\frac{\partial^2 T}{\partial(\bar{x}+c\bar{t})^2} + \frac{\partial^2 T}{\partial \bar{y}^2}\right)\right] + \frac{\partial \bar{q}_r}{\partial \bar{y}} + Q_0 \tag{23}$$

$$\frac{\partial C}{\partial \bar{t}} + (\bar{u}+c)\frac{\partial C}{\partial(\bar{x}+c\bar{t})} + \bar{v}\frac{\partial C}{\partial \bar{y}} = D\left[\left(\frac{\partial^2 C}{\partial(\bar{x}+c\bar{t})^2} + \frac{\partial^2 C}{\partial y}\right)\right] + \frac{DK_T}{T_m}\left[\left(\frac{\partial^2 T}{\partial(\bar{x}+c\bar{t})^2} + \frac{\partial^2 T}{\partial \bar{y}^2}\right)\right] \tag{24}$$

To simplify the governing equations, the next dimensionless quantities are introduced

$$\left.\begin{aligned} x = \frac{\bar{x}}{\lambda} \ , \ y = \frac{\bar{y}}{d_1} \ , \ t = \frac{c\bar{t}}{\lambda}, u = \frac{\bar{u}}{c} \ , \ v = \frac{\lambda \bar{v}}{d_1 c} \ , \ p = \frac{{d_1}^2 \bar{p}}{c\lambda\mu_0} \\ h_1 = \frac{\bar{h}_1}{d_1} \ , \ h_2 = \frac{\bar{h}_2}{d_1} \ , \ a = \frac{a_1}{d_1} \ , \ b = \frac{a_2}{d_1} \ , \ d = \frac{d_2}{d_1} \\ \mu(\theta) = \frac{\bar{\mu}(T)}{\mu_0}, \theta = \frac{(T-T_0)}{\Delta T} \ , \phi = \frac{(C-C_0)}{\Delta C} \ , \ \delta = \frac{d1}{\lambda} \ , m = \frac{\bar{m}\lambda}{d_1} \end{aligned}\right\} \tag{25}$$

Where $x, y, t, u, v, p,$ a, b, $\theta, \phi, \delta, m$ are the components of the dimensionless coordinates ,the dimensionless time, the dimensionless axial velocity, the dimensionless transverse component of velocity, the dimensionless pressure, the amplitudes of the lower wall, the amplitudes of the upper wall, the dimensionless viscosity, the dimensionless temperature, the dimensionless concentration, the wave number, and the non-uniform parameter, respectively. $\Delta C = (C_1 - C_0)$ and $\Delta T = (T_1 - T_0)$ denote the mass concentration difference and temperature difference, respectively.

Also, we shall make use of several dimensionless parameters that are registered below:

$$\left.\begin{aligned} Gr = \frac{\rho g d_1^2 (\Delta T)\alpha_1}{c\mu_0}, Gm = \frac{\rho g d_1^2 (\Delta T)\alpha_2}{c\mu_0}, \ M^2 = \frac{\beta_0^2 d_1^2 \sigma}{\mu_0}, \beta = \frac{{d_1}^2 Q_0}{(\Delta T)\kappa}, Re = \frac{\rho d_1 2c}{\mu_0} \\ K = \frac{K_0}{{d_1}^2} \ , \ \mathrm{Sr} = \frac{\rho D K_T T_0}{\mu_0 T_m (C - C_0)} \ , \mathrm{Sc} = \frac{\mu_0}{\rho D} \ , \mathrm{Nr} = \frac{16\sigma' T_0^3}{3k' d_1 \kappa} \ , \mathrm{Pr} = \frac{\mu_0 C_p}{\kappa} \end{aligned}\right\} \tag{26}$$

where $Gr$ and $Gm$ are called the Grashof number which stands for the solute Grashof number, $M$ is the Hartmann number, $\beta$ is the heat source / sink parameter, $Re$ is the Reynolds number, $K$ is the Darcy number, $Sr$ is the Soret number which represents the thermal diffusion effect, $Sc$ is the Schmidt number, $Nr$ is the thermal radiation parameter, and $Pr$ is the Prandtl number.

By using the dimensionless quantities in (25) and (26), with the flow being steady, the equations (20 ) to (24 ) become

$$\frac{\partial u}{\partial x} + \frac{\partial v}{\partial y} = 0 \tag{27}$$

$$Re.\delta\left[(u+1)\frac{\partial u}{\partial x}+v\frac{\partial u}{\partial y}\right]=-\frac{\partial p}{\partial x}+2\delta^2\frac{\partial}{\partial x}\left[\mu(\theta)\frac{\partial u}{\partial x}\right]+\frac{\partial}{\partial y}\left[\mu(\theta)\left(\delta^2\frac{\partial v}{\partial x}+\frac{\partial u}{\partial y}\right)\right]-M^2(u+1)+$$
$$Gr.\theta.\sin(\xi)+Gm.\phi.\sin(\xi)-\frac{\mu(\theta)}{k}(u+1) \quad (28)$$

$$Re.\delta^3\left[(u+1)\frac{\partial v}{x}+v\frac{\partial v}{\partial y}\right]=-\frac{\partial p}{\partial y}+2\delta^2\frac{\partial}{\partial y}\left[\mu(\theta)\frac{\partial v}{\partial y}\right]+\frac{\partial}{\partial x}\delta^2\left[\mu(\theta)\delta^2\left(\frac{\partial v}{\partial x}+\frac{\partial u}{\partial y}\right)\right]-\delta^2\frac{\mu(\theta)}{k}v \quad (29)$$

$$Re.\delta.Pr\left[(u+1)\frac{\partial\theta}{\partial x}+v\frac{\partial\theta}{\partial y}\right]=\left[\delta^2\frac{\partial^2\theta}{\partial x^2}+\frac{\partial^2\theta}{\partial y^2}\right]+Nr\frac{\partial^2\theta}{\partial y^2}+\Delta T.\beta \quad (30)$$

$$Re.\delta\left[(u+1)\frac{\partial\phi}{\partial x}+v\frac{\partial\phi}{\partial y}\right]=\frac{1}{Sc}\left[\delta^2\frac{\partial^2\phi}{\partial x^2}+\frac{\partial^2\phi}{\partial y^2}\right]+Sr\left[\delta^2\frac{\partial^2\theta}{\partial x^2}+\frac{\partial^2\theta}{\partial y^2}\right] \quad (31)$$

The stream function $\psi(x, y, t)$ and its relationship with velocity components is defined below

$$u=\frac{\partial\psi}{\partial y} \text{ and } \quad v=-\frac{\partial\psi}{\partial x} \quad (32)$$

Now, by the long wavelength approximation $\delta(\delta \ll 1)$ and considering low Reynolds number $(Re \to 0)$ , the Eqs. (27)-(31) become

$$\frac{\partial\psi}{\partial x\partial y}-\frac{\partial\psi}{\partial y\partial x}=0 \quad (33)$$

$$\frac{\partial p}{\partial x}=\frac{\partial}{\partial y}\left[\mu(\theta)\frac{\partial^2\psi}{\partial y^2}\right]-M^2\left(\frac{\partial\psi}{\partial y}+1\right)+Gr.\theta.\sin(\xi)+Gm.\phi.\sin(\xi)-\frac{\mu(\theta)}{k}\left(\frac{\partial\psi}{\partial y}+1\right) \quad (34)$$

$$\frac{\partial p}{\partial y}=0 \quad (35)$$

$$(Nr+1)\frac{\partial^2\theta}{\partial y}+\beta=0 \quad (36)$$

$$\frac{1}{Sc}\left[\frac{\partial^2\phi}{\partial y^2}\right]+Sr\left[\frac{\partial^2\theta}{\partial y^2}\right]=0 \quad (37)$$

For the ease of investigation, most studies on fluid mechanics take fluid with a constant viscosity . But in several processes, the viscosity is a function of heat, and out of several variations of viscosity with non-dimensional temperature, the following form was proposed by Slattery [21].

$\mu(\theta)=e^{-\alpha\theta}$ or $\mu(\theta)=1-\alpha\theta$ where $\alpha \ll 1$ . (38)

where ($\alpha$) is the viscosity parameter, which is a constant. Results for the constant viscosity are obtained for $=0$ .

By the aid of Eq.(38) , the dimensionless Eq.(34) will be

$$\frac{\partial p}{\partial x}=\frac{\partial}{\partial y}\left[(1-\alpha\theta)\frac{\partial^2\psi}{\partial y^2}\right]-M^2\left(\frac{\partial\psi}{\partial y}+1\right)+Gr.\theta.\sin(\xi)+Gm.\phi.\sin(\xi)-\frac{(1-\alpha\theta)}{k}\left(\frac{\partial\psi}{\partial y}+1\right) \quad (39)$$

Eq.(35) shows that the pressure is independent of the dimensionless coordinate ( $y$ ) . By combining Eqs. (35) & (39) and after removing the pressure, we get the following

$$0=(1-\alpha\theta)\frac{\partial^4\psi}{\partial y^4}-2\alpha\frac{\partial\theta}{\partial y}\frac{\partial^3\psi}{\partial y^3}-\alpha\frac{\partial^2\theta}{\partial y^2}\frac{\partial^2\psi}{\partial y^2}-\left(N^2-\frac{1}{k}\alpha\theta\right)\frac{\partial^2\psi}{\partial y^2}+\frac{\alpha}{k}\frac{\partial\theta}{\partial y}\left(\frac{\partial\psi}{\partial y}+1\right)+Gr.\frac{\partial\theta}{\partial y}.\sin(\xi)+$$
$$Gm.\frac{\partial\phi}{\partial y}.\sin(\xi) \quad (40)$$

$$N^2=M^2+\frac{1}{k}$$

The suitable boundary conditions in non-dimensional wave frame are

Model-1:

$$\psi=\frac{F}{2} \ , \ \frac{\partial\psi}{\partial y}+\beta_1\frac{\partial^2\psi}{\partial y^2}=-1 \ , \ \theta=1 \ , \ \phi=1 \quad at \ \ y=h_1 \quad (41)$$

$$\psi=-\frac{F}{2} \ , \ \frac{\partial\psi}{\partial y}-\beta_1\frac{\partial^2\psi}{\partial y^2}=-1 \ , \ \theta=0 \ , \ \phi=0 \quad at \ \ y=h_2 \quad (42)$$

Model-2 :

$$\psi=\frac{F}{2} \ , \ \frac{\partial\psi}{\partial y}=0 \ , \ \theta=1 \ , \ \phi=1 \quad at \ \ y=h_1 \quad (43)$$

$$\psi=-\frac{F}{2} \ , \ \frac{\partial\psi}{\partial y}=0 \ , \ \theta=0 \ , \ \phi=0 \quad at \ \ y=h_2 \quad (44)$$

where $\beta_1=\frac{\beta_0}{d_1}$ is the non-dimensional velocity-slip parameter and ($F$ ) is the non-dimensional mean flow rate in the wave frame.

The non-dimensional forms of the lower and upper walls are

$$h_1(x)=1+m(t+x)+a\,Cos(2\pi x) \quad (45)$$

$$h_2(x)=-d-m(t+x)-b\,Cos(2\pi x+\varphi) \quad (46)$$

Also the Eq.(3) in the dimensionless frame is

$$a^2+b^2+2abCos(\varphi)\leq(1+d)^2 \quad (47)$$

**5- Rate of Volume Flow**

The instantaneous volume flow rate in the laboratory frame of reference is defined as

$$\bar{Q} = \int_{\bar{h}_1(\bar{x},\bar{t})}^{\bar{h}_2(\bar{x},\bar{t})} \bar{U}(\bar{X},\bar{Y},\bar{t})\, d\bar{Y} \tag{48}$$

Likewise , the rate of volume flow in the wave frame is obtained as

$$\bar{q} = \int_{\bar{h}_1(\bar{x},\bar{t})}^{\bar{h}_2(\bar{x},\bar{t})} \bar{u}(\bar{x},\bar{y}) d\bar{y} \tag{49}$$

Using the conversions (19) in (48), and with (49), we obtain the connection between the volumetric flow rates as follows

$$\bar{Q} = \bar{q} + c\big(\bar{h}_1(\bar{x},\bar{t}) - \bar{h}_2(\bar{x},\bar{t})\big) \tag{50}$$

The mean flow over a period of time $T = (\frac{\lambda}{c})$ at a fixed position $x$ is given by

$$\tilde{Q} = \frac{1}{T}\int_0^T \bar{Q}\, dt \tag{51}$$

By substituting (50) into (51), we have

$$\tilde{Q} = q + c(d_1 + d_2) + 2.m.\bar{x} \tag{52}$$

Let $(Q)$ be the dimensionless time mean flow, where

$$F = \frac{q}{cd_1} \text{and } Q = \frac{\bar{Q}}{cd_1} \tag{53}$$

The dimensionless form of (48) is

$$Q = \int_{h_1}^{h_2} u\, dy \tag{54}$$

We derive the next relations by using (52)

$$Q = F + 1 + d + 2m \tag{55}$$

and

$$F = \int_{h_1(x)}^{h_2(x)} \frac{\partial \psi}{\partial y} dy = \psi(h_2) - \psi(h_1) \tag{56}$$

**6- Solutions of The Temperature and Concentration Equations**

We obtain the exact solution for the temperature Eq.(36), satisfying the boundary conditions (41) & (42), by the following

$$\theta = -\frac{\beta y^2}{2(1+Nr)} + C_1 + yC_2 \tag{57}$$

where

$$C_1 = -\frac{2h_2+\beta h_1^2 h_2-\beta h_1 h_2^2+2h_2 Nr}{2(h_1-h_2)(1+Nr)}$$

$$C_2 = -\frac{2+Bh_1^2-Bh_2^2+2Nr}{2(-h_1+h_2)(1+Nr)}$$

While the solution of the concentration Eq. (37), with boundary conditions (41 ) & (42), is given by

$$\phi_1 = \frac{ScSry^2\beta}{2(1+Nr)} + C_3 + yC_4 \tag{58}$$

where

$$C_3 = -\frac{2h_2+2h_2Nr-\beta {h_1}^2 h_2 ScSr+\beta h_1 {h_2}^2 ScSr}{2(h_1-h_2)(1+Nr)}$$

$$C_4 = -\frac{2+2Nr-\beta {h_1}^2 ScSr+\beta {h_2}^2 ScSr}{2(-h_1+h_2)(1+Nr)}$$

**7- The Perturbation Technique**

The momentum equation (40) is non-linear. For arbitrary values of the parameters contained in this equation, the exact solution appears very impossible to obtain. However, the viscosity parameter $(\alpha)$ is very small. Therefore, the consideration is concentrated to the perturbation technique for a small fluid parameter $(\alpha)$ . For that, we can widen the stream function $(\psi)$ , pressure ($P$), and the flow rate ($F$) in a power series form, as follows

$$\left.\begin{aligned} \psi &= \psi_0 + \alpha\psi_1 + \alpha^2\psi_2 + \cdots \\ P &= P_0 + \alpha P_1 + \alpha^2 P_2 + \cdots \\ F &= F_0 + \alpha F_1 + \alpha^2 F_2 + \cdots \end{aligned}\right\} \tag{59}$$

By substituting Eq.(59) into Eqs.(39) & (40) and then comparing the coefficients of the same power of up to the first order, we get the following two system zeroth-order and first-order equations:

**7.1- Zeroth Order System**

$$\frac{\partial p_0}{\partial x}=\frac{\partial^3\psi_0}{\partial y^3}-M^2\left(\frac{\partial\psi_0}{\partial y}+1\right)-Gr.\theta.\sin(\xi)-Gm.\phi.\sin(\xi)-\frac{(1-\alpha\theta)}{k}\left(\frac{\partial\psi_0}{\partial y}+1\right) \quad (60)$$

$$0=\frac{\partial^4\psi_0}{\partial y^4}-(N^2)\frac{\partial^2\psi_0}{\partial y^2}+Gr.\frac{\partial\theta}{\partial y}.\sin(\xi)+Gm.\frac{\partial\phi}{\partial y}.\sin(\xi) \quad (61)$$

with boundary conditions

Model-1:

$$\left.\begin{aligned}\psi_0=\tfrac{F_0}{2}\quad,\quad \frac{\partial\psi_0}{\partial y}+\beta_1\frac{\partial^2\psi_0}{\partial y^2}=-1\,,\ \theta=1\ ,\phi=1\quad at\quad y=h_1\\ \psi_0=-\tfrac{F_0}{2}\ ,\ \frac{\partial\psi_0}{\partial y}-\beta_1\frac{\partial^2\psi_0}{\partial y^2}=-1\,,\ \theta=0\ ,\phi=0\quad at\quad y=h_2\end{aligned}\right\} \quad (62)$$

Model-2:

$$\left.\begin{aligned}\psi_0=\tfrac{F_0}{2}\quad,\quad \frac{\partial\psi_0}{\partial y}=0\,,\ \theta=1\ ,\ \phi=1\quad at\quad y=h_1\\ \psi_0=-\tfrac{F_0}{2}\quad,\quad \frac{\partial\psi_0}{\partial y}=0\,,\ \theta=0\,,\ \phi=0\quad at\quad y=h_2\end{aligned}\right\} \quad (63)$$

By solving the Eq.(61) for Model-1, the final solution for the zeroth order is

$$\psi_0=\mathrm{C}_7+\mathrm{y}C_8\frac{2e^{Ny}\mathrm{C}_5+2e^{-Ny}\mathrm{C}_6+(\mathrm{C}_4\mathrm{Gm}+\mathrm{C}_2\mathrm{Gr})y^2\mathrm{Sin}(\xi)-\frac{B(\mathrm{Gr}-\mathrm{Gmscsr})y^3\mathrm{Sin}(\xi)}{3(1+\mathrm{Nr})}}{2N^2} \quad (64)$$

**7.2- First Order System**

The complemented first order perturbation system is found in the next form

$$\frac{\partial p_1}{\partial x}=\frac{\partial^3\psi_1}{\partial y^3}-\theta\frac{\partial^3\psi_0}{\partial y^3}-\frac{\partial\theta}{\partial y}\frac{\partial^2\psi_0}{\partial y^2}-N^2\frac{\partial\psi_1}{\partial y}+\frac{\theta}{K}\left(\frac{\partial\psi_0}{\partial y}+1\right) \quad (65)$$

$$0=\frac{\partial^4\psi_1}{\partial y^4}-\theta\frac{\partial^4\psi_0}{\partial y^4}-2\frac{\partial\theta}{\partial y}\frac{\partial^3\psi_0}{\partial y^3}-\frac{\partial^2\theta}{\partial y^2}\frac{\partial^2\psi_0}{\partial y^2}-(N^2)\frac{\partial^2\psi_1}{\partial y^2}+\frac{\theta}{K}\frac{\partial^2\psi_0}{\partial y^2}+\frac{1}{K}\frac{\partial\theta}{\partial y}\left(\frac{\partial\psi_0}{\partial y}+1\right) \quad (66)$$

with boundary conditions

Model-1:

$$\left.\begin{aligned}\psi_1=\tfrac{F_1}{2}\quad,\quad \frac{\partial\psi_1}{\partial y}+\beta_1\frac{\partial^2\psi_1}{\partial y^2}=0\,,\ \theta=1\ ,\phi=1\quad at\quad y=h_1\\ \psi_1=-\tfrac{F_1}{2}\ ,\ \frac{\partial\psi_1}{\partial y}-\beta_1\frac{\partial^2\psi_1}{\partial y^2}=0\,,\ \theta=0\ ,\phi=0\quad at\quad y=h_2\end{aligned}\right\} \quad (67)$$

Model-2:

$$\left.\begin{aligned}\psi_1=\tfrac{F_1}{2}\quad,\quad \frac{\partial\psi_1}{\partial y}=0\,,\ \theta=1\ ,\phi=1\quad at\quad y=h_1\\ \psi_1=-\tfrac{F_1}{2}\ ,\ \frac{\partial\psi_1}{\partial y}=0\,,\ \theta=0\ ,\phi=0\quad at\quad y=h_2\end{aligned}\right\} \quad (68)$$

The first order solution gained from the above system is

$$\psi_1=a_3+ya_4+\frac{1}{48kN^6(1+Nr)^2}(e^{-Ny}(1+Nr)(\beta(C_6(-45-42Ny-18N^2y^26Ny+6N^2y^2+4N^3y^3))-e^{Ny}(8(1+C_8)N^4y^3+C_5e^{Ny}(45-42Ny+18N^2y^2-4N^3y^3+kN^2(-3+6Ny-6N^2y^2+4N^3y^3))))+6N(1+Nr)(-2C_1N(-1+kN^2)(-C_5e^{2Ny}(-5+2Ny)+C_6(5+2Ny))+C_2(C_6(7+6Ny+2N^2y^2+kN^2(3-2Ny-2N^2y^2))+e^{Ny}(4(1+C_8)N^3y^2+C_5e^{Ny}(-7+6Ny-2N^2y^2+kN^2(-3-2Ny+2N^2y^2))))+8kN^3(e^{2Ny}a_1+a_2)))-\frac{2}{5}y^2(-20(C_4Gm+C_2Gr)N^2(1+Nr)^2(3C_1+2C_2y)-6\beta^2(Gr-GmScSr)y(20-10kN^2+N^2y^2)+5\beta(1+Nr)(4C_1N^2(Gr-GmScSr)y-3C_2GmScSr(12-8kN^2+N^2y^2)+6C_2Gr(12-6kN^2+N^2y^2)+3C_4Gm(12-4kN^2+N^2y^2)))Sin[\xi]) \quad (69)$$

The values of coefficients $(C_5, C_6, C_7, C_8, a_1, a_2, a_3, a_4)$ are large non-constant and their values can be calculated with the boundary conditions in Eq.(67) by using Mathematica 11 programs. Also, these coefficients are changing when we use the no-slip conditions in Eqs.(63) & (68).

**8- Results and Discussion**

This section is devoted to study the influences of different parameters on the axial velocity for both models, i.e., temperature distribution, concentration distribution, and pressure gradient. The results are described by the graphical clarifications while Mathematica program was used to obtain results. The trapping phenomenon was also studied for the slip condition through graphs.

**8.1- Velocity Profile**

The axial velocity is calculated at the $(x = 0.7)$ cross-section in the cases of slip and no-slip conditions of the channel, which are compared based on differences in physical parameters such as Grashof number (Gr) , the non-uniform parameter (m), the solute Grashof number (Gm) , Hartman number (M), and mean flow rate $(Q)$, via Figures -(1-5).

Figure-1 provides an idea of the difference in the axial velocity that takes place with the variation in the Grashof number (Gr). When the value of (Gr) is increased, the velocity profile is progressively reduced down to a definite point which is called the point of inflexion. Next to this point , the orientation is reflected, where with the augmentation of (Gr) , the velocity progressively increases, with the observation that the velocity profile does not change near the walls of the channel for model-1. Whereas the velocity increases up to the point of inflexion at ( $y = -1.61$ ). Following this point, the velocity decreases down to another point of inflexion at ( $y = -0.44$ ), then it increases again and also notices that the velocity profile does not change near the walls of the channel for model -2. the measures of the velocity close in on a specific value at some point of the upper wall of the channel for model -2. The influence of the non-uniform parameter (m) on the axial velocity is presented in Figure-2. We observed that the velocity distribution decreases in the middle of the channel by increasing the non-uniform parameter, with the note that the velocity increases near the walls channel for both model, Figure-3 denotes that in both model, the axial velocity decreases in a part of the channel but it increases in another part with increasing the value of (Gm). Figure-4 exhibits the variation in the axial velocity with the alteration in the value of (M) for both models. It is important to note the decrease in the velocity near the center of channel (for $-0.575 \le y \le 0.898$) and the increase in the remaining intervals with the increase of (M) for model-1. While in model -2 , we observed the existence of two points of inflexion. It may be also noted that the orientation of velocity is reversed after passing the point of inflexion and that the measures of the velocity converge to a specific value at some point of the upper wall. These results appear as factual because the magnetic field acts in the transverse trend to the flow and the magnetic force resists the flow. The influence of the parameter (Q) on the velocity profile is shown in Figure-5. We observed that the velocity distribution increases with increasing the mean flow rate (Q) for model-1, whereas, for model-2, the velocity increases in the middle of the channel and decreases near the walls with increasing (Q).

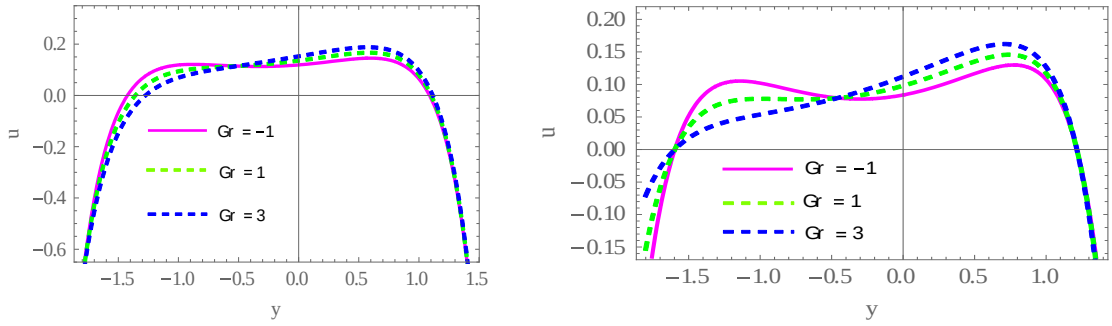


Model-1: slip Model-2: no-slip

**Figure 1**-The effect of (Gr) on velocity profile at $a = 0.5, b = 0.5, \varphi = \mathrm{Pi}/4, t = 0.3, m = 0.1, Q = 2.4, \beta_1 = 0.5, \zeta = \mathrm{Pi}/4, k = 1.5, \alpha = 0.05, \mathrm{Nr} = 0.8, \beta = 1, M = 4, d = 1$ , $\mathrm{Sc} = 2, \mathrm{Sr} = 3, \mathrm{Gm} = 2$.

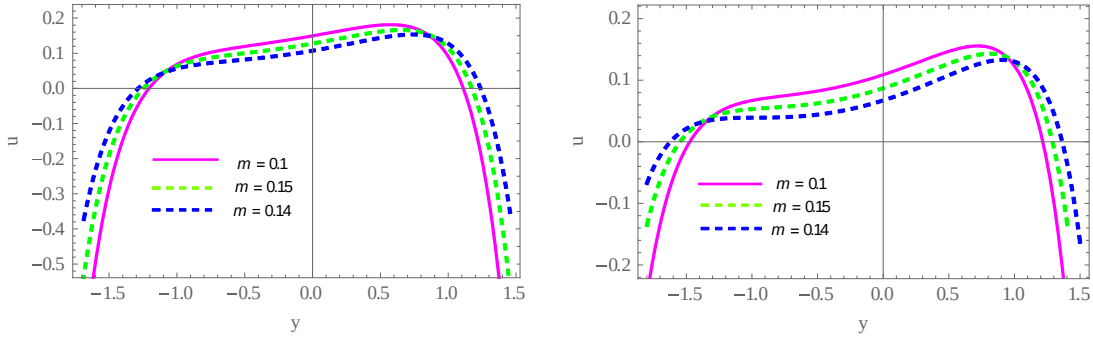


Model-1: slip Model-2: no-slip

**Figure 2**-The effect of (m) on velocity profile at $a = 0.5, b = 0.5, \varphi = \mathrm{Pi}/4, t = 0.3, Nr = 0.8, Q = 2.4, \beta_1 = 0.5, \zeta = \mathrm{Pi}/4, k = 1.5, \mathrm{Gr} = 2, \alpha = 0.05, \beta = 1, M = 4, d = 1$ , $\mathrm{Sc} = 2, \mathrm{Sr} = 3,$ $\mathrm{Gm} = 2.$

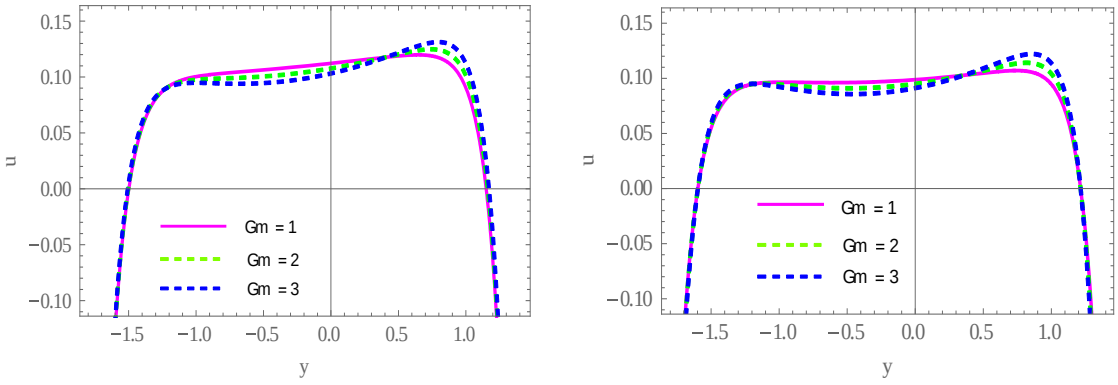


Model-1: slip Model-2: no-slip

**Figure 3**-The effect of (Gm) on velocity profile at $a = 0.5, b = 0.5, \varphi = \mathrm{Pi}/4, t = 0.3, m = 0.1, Q = 2.4, \beta_1 = 0.5, \zeta = \mathrm{Pi}/4, k = 1.5, \mathrm{Gr} = 2, \mathrm{Nr} = 0.8, \beta = 1, M = 4, d = 1$ , $\mathrm{Sc} = 2, \mathrm{Sr} = 3,$ $\alpha = 0.5.$

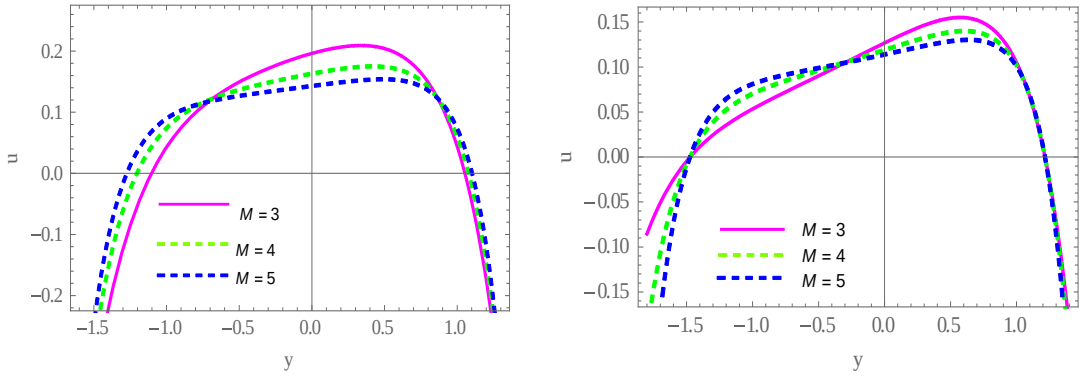


Model-1: slip Model-2: no-slip

**Figure 4**-The effect of (M) on velocity profile at $a = 0.5, b = 0.5, \varphi = \mathrm{Pi}/4, t = 0.3, m = 0.1, Q = 2.4, \beta_1 = 0.5, \zeta = \mathrm{Pi}/4, k = 1.5, \mathrm{Gr} = 2, \mathrm{Nr} = 0.8, B = 1, \alpha = 0.05, d = 1$ , $\mathrm{Sc} = 2, \mathrm{Sr} = 3,$ $\mathrm{Gm} = 2.$

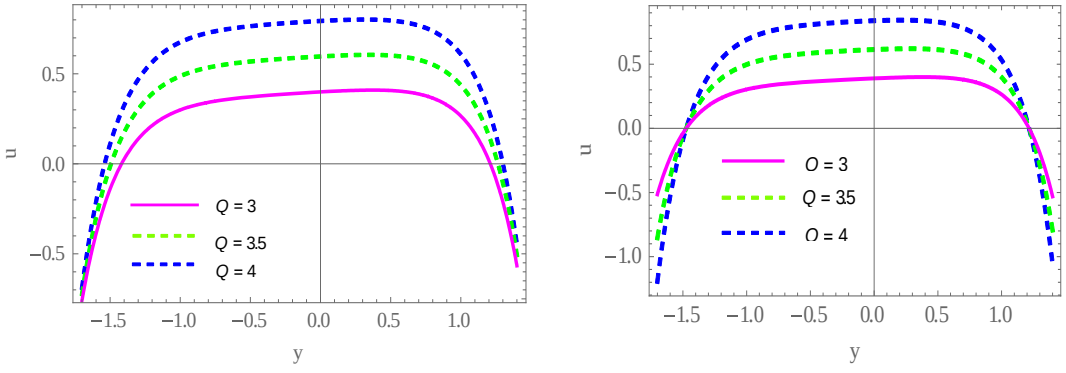


Model-1: slip Model-2: no-slip

**Figure 5**-The effect of (Q) on velocity profile at $a = 0.5, b = 0.5, \varphi = \mathrm{Pi}/4, t = 0.3, m = 0.1, M = 4, \beta_1 = 0.5, \zeta = \mathrm{Pi}/4, k = 1.5, \mathrm{Gr} = 2, \mathrm{Nr} = 0.8, \beta = 1, \alpha = 0.05, d = 1$ , $\mathrm{Sc} = 2, \mathrm{Sr} = 3,$ $\mathrm{Gm} = 2.$

**8.2- Temperature Profile**

Figures-(6-10) depict the impacts of heat transfer on the peristaltic flow for several values of parameters. The plots provide important information that deal with the heat transference in the fluid. Fig. 6 demonstrates the effects of the heat source / sink parameter ($\beta$) on the temperature distribution. The graphical results show that the temperature increases with the increase in the heat generation

parameter. However, the scheme presented in Figure- 7 points to an adverse direction, where the value of the thermal radiation parameter $(Nr)$ is increased. This figure shows that the temperature distribution is greatly influenced by $(Nr)$. Here we can make an important remark that the temperature is reduced with the increase in thermal radiation. Further, Figs. 8-10 demonstrate the effects of the phase difference $(\varphi)$ , the amplitude of the upper wall $(b)$. and the amplitude of the lower wall $(a)$ on the temperature distribution. It can be observed that the temperature distribution increases with increasing $(\varphi)$ and $(b)$. The temperature differs significantly at the lower wall and middle part, while an increase in the amplitude of the lower wall $(a)$ enhances the temperature distribution at the upper wall as well as in the center of the channel.

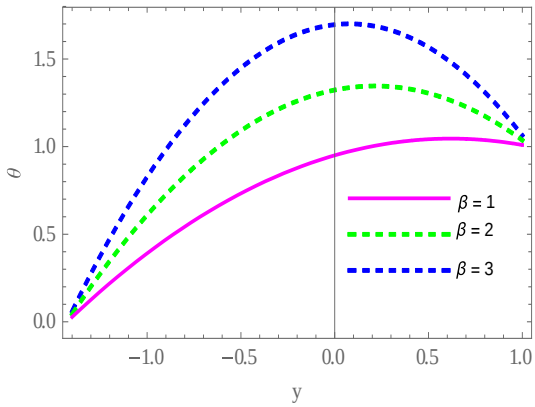


**Figure 6**-The effect of $(\beta)$ on temperature profile at $x = 1.7, a = 0.5, b = 0.5, \varphi = \pi/4, t = 0.3, m = 0.1, \mathrm{Nr} = 1, d = 1.$

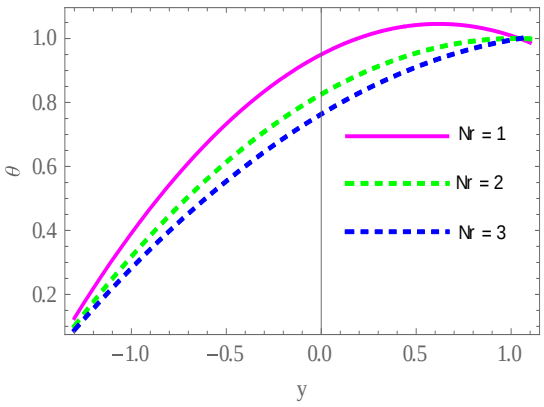


**Figure7**-The effect of $(\beta)$ on temperature profile at $x = 1.7, a = 0.5, b = 0.5, \varphi = \pi/4, t = 0.3, m = 0.1, \beta = 1, d = 1.$

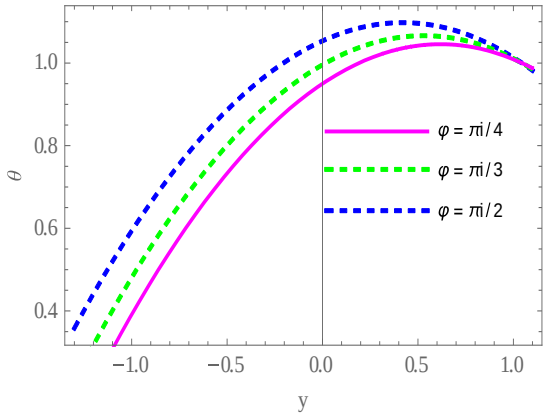


**Figure 8**-The effect of $(\varphi)$ on temperature profile at $x = 1.7, a = 0.5, b = 0.5, t = 0.3, m = 0.1, \mathrm{Nr} = 1, \beta = 1, d = 1.$

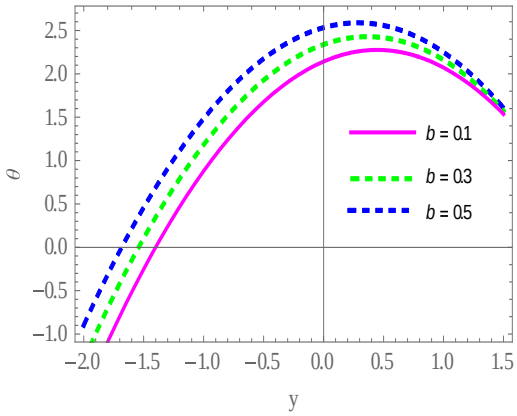


**Figure 9**-The effect of (b) on temperature profile at $x = 1.7, a = 0.5, t = 0.3, m = 0.1, \mathrm{Nr} = 1, \beta = 1, d = 1, \varphi = \pi/4.$

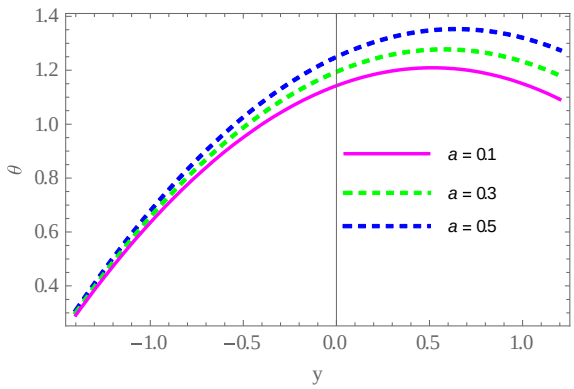


**Figure 10**-The effect of $(a)$ on temperature profile at $x = 1.7, b = 0.5, t = 0.3, m =$

$0.1, \mathrm{Nr} = 1, \beta = 1, d = 1, \varphi = \pi/4.$

**8.3- Concentration Profile**

Figures-(11-16) are plotted to illustrate the effects of different parameters on the concentration profile. In Figures-(11-13), it is noticed that the concentration profile decreases with the increase in Schmidt number (Sc), Soret number (Sr) and the heat source / sink parameter ($\beta$). From Figure-14, it is obvious that the concentration profile increases with increasing the thermal radiation parameter (Nr) . Also, the effect of the non-uniform parameter (m) on the concentration is shown in Figure-15 .It can be noted that the concentration profile decreases with increasing (m) towards the upper wall of the channel. While Figure-16 demonstrates that the concentration profile increases in the boundary layer and progressively decreases upon approaching the upper wall with increasing the phase difference ($\varphi$).

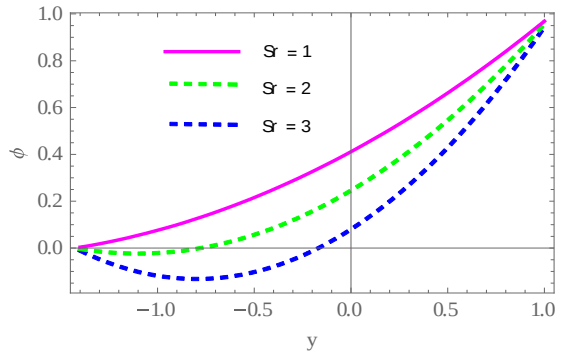


**Figure 11**-The effect of ($Sr$) on concentration profile at $x = 1.7, a = 0.5, b = 0.5, t = 0.3, m = 0.1, \mathrm{Nr} = 0.8, \beta = 1, d = 1, Sc = 0.2, , \varphi = \pi/4.$

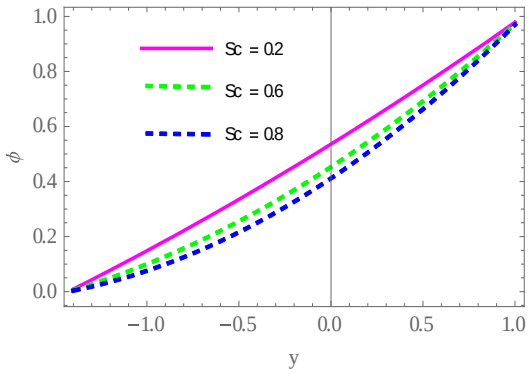


**Figure 12**-The effect of ($Sc$) on concentration profile at $x = 1.7, a = 0.5, b = 0.5, t = 0.3, m = 0.1, \mathrm{Nr} = 0.8, \beta = 1, d = 1 \ , Sr = 0.5, , \varphi = \pi/4.$

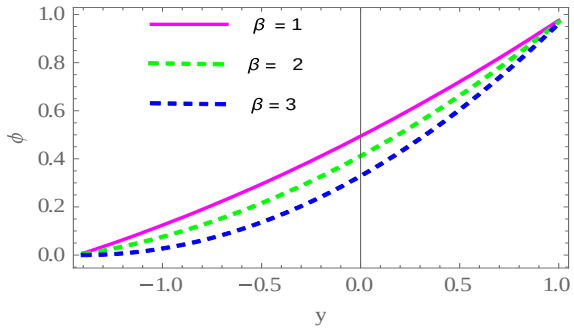


**Figure 13**-The effect of (β) on concentration profile at $x = 1.7, a = 0.5, b = 0.5, t = 0.3, m = 0.1, \mathrm{Nr} = 0.8, d = 1, Sc = 0.4, Sr = 0.5, , \varphi = \pi/4$

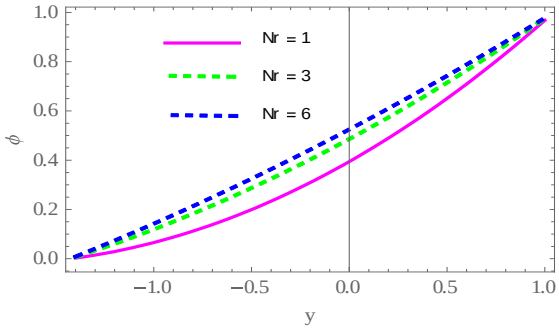


**Figure 14**-The effect of ($Nr$) on concentration profile at $x = 1.7, a = 0.5, b = 0.5, t = 0.3, m = 0.1, \beta = 1, d = 1, Sc = 0.4, Sr = 0.5, , \varphi = \pi/4$

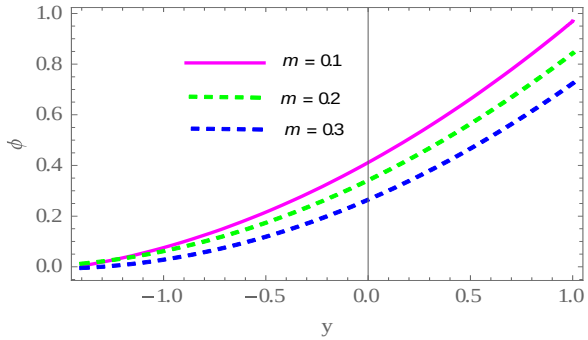


**Figure 15**-The effect of (m) on concentration profile at $x = 1.7, a = 0.5, b = 0.5, t = 0.3, \beta =$

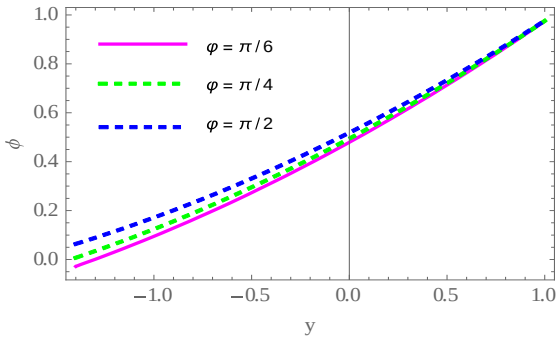


**Figure 16**-The effect of ($\varphi$) on concentration profile at $x = 1.7, a = 0.5, b = 0.5, t =$

$1, \mathrm{Nr} = 0.8, d = 1, Sc = 0.4, Sr = 0.5, \varphi = \pi/4.$ $0.3, m = 0.1, \mathrm{Nr} = 0.8, d = 1, Sc = 0.4, Sr = 0.5, \beta = 1.$

**8.4- Pressure Gradient Profile**

Figures-(17-21) show the alteration of pressure gradient against the axial coordinate x for various wave forms. The impacts of Gr, (Gm) and the heat source / sink parameter ($\beta$) on pressure gradient are exhibited in Figures-(17-19). It can be observed from Figure-17 that increasing Grashof number increases the pressure gradient. It is also noticed that increasing (Gm) and ($\beta$) increases the pressure gradient. In Figures-(20 & 21), it is illustrated that increasing the Soret number (Sr) and Schmidt number (Sc) leads to decreased pressure gradient . It is noted that, in the wider part of the channels $x \in [0, 0.2]$ and $x \in [0.7, 1]$, the pressure gradient is low, so that the flow can be simply passed without the imposition of high pressure gradient. However, in the tight part of the channel $x \in [0.2, 0.7]$, the pressure gradient is high, that is, a much higher pressure gradient is needed to preserve the same given volume of flow rate.

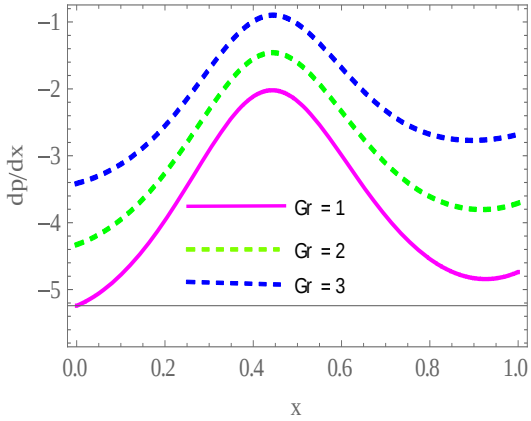


**Figure 17**-The effect of (Gr) on the pressure gradient profile at $a = 0.5, b = 0.5, \varphi = \mathrm{Pi}/4, t = 0.3, m = 0.1, Q = 2.4, \beta_1 = 0.5, \zeta = \mathrm{Pi}/4, k = 1.5, \alpha = 0.05, \mathrm{Nr} = 0.8, B = 1, M = 4, d = 1$ , $\mathrm{Sc} = 2, \mathrm{Sr} = 3, \mathrm{Gm} = 2.$

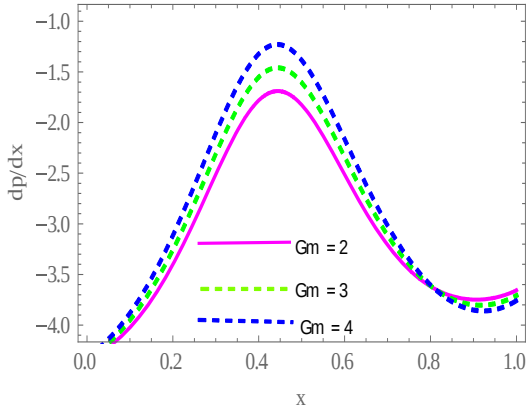


**Figure 18**-The effect of (Gm) on the pressure gradient profile at $a = 0.5, b = 0.5, \varphi = \mathrm{Pi}/4, t = 0.3, m = 0.1, Q = 2.4, \beta_1 = 0.5, \zeta = \mathrm{Pi}/4, k = 1.5, \mathrm{Gr} = 2, \mathrm{Nr} = 0.8, B = 1, M = 4, d = 1$ , $\mathrm{Sc} = 2, \mathrm{Sr} = 3, \alpha = 0.5.$

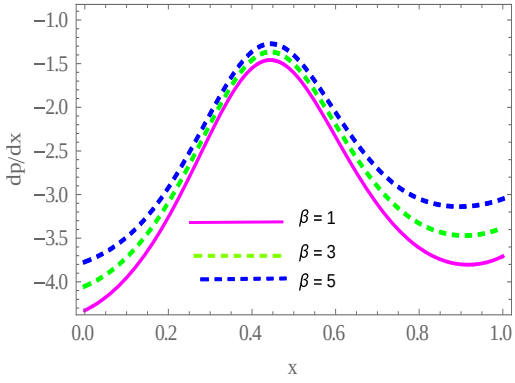


**Figure 19**-The effect of ($\beta$) on the pressure gradient profile at $a = 0.5, b = 0.5, \varphi = \mathrm{Pi}/4, t = 0.3, m = 0.1, Q = 2.4, \beta_1 = 0.5, \zeta = \mathrm{Pi}/4, k = 1.5, \alpha = 0.05, \mathrm{Nr} = 0.8, Gr = 2, M = 4, d = 1$ , $\mathrm{Sc} = 2, \mathrm{Sr} = 3, \mathrm{Gm} = 2.$

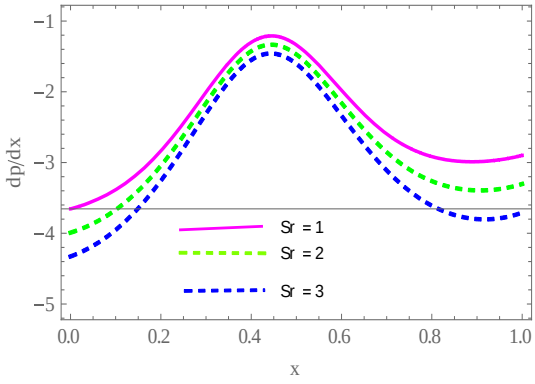


**Figure 20**-The effect of (Sr) on the pressure gradient profile at $a = 0.5, b = 0.5, \varphi = \mathrm{Pi}/4, t = 0.3, m = 0.1, Q = 2.4, \beta_1 = 0.5, \zeta = \mathrm{Pi}/4, k = 1.5, \alpha = 0.05, \mathrm{Nr} = 0.8, B = 1, Gr = 2, d = 1$ , $\mathrm{M} = 4, \mathrm{Sr} = 3, \mathrm{Gm} = 2.$

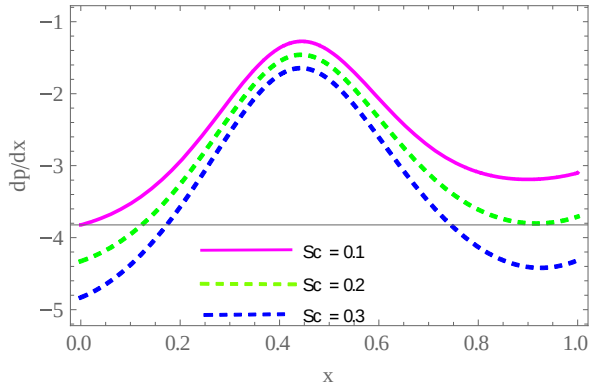


**Figure 21**-The effect of (Sc) on the pressure gradient profile at $a = 0.5, b = 0.5, \varphi = \mathrm{Pi}/4, t = 0.3, m = 0.1, Q = 2.4, \beta_1 = 0.5, \zeta = \mathrm{Pi}/4, k = 1.5, \alpha = 0.05, \mathrm{Nr} = 0.8, B = 1, M = 4, d = 1$ , $\mathrm{Gr} = 2, \mathrm{Sr} = 3,\ \mathrm{Gm} = 2.$

**8.5- Trapping**

Trapping is also an important phenomenon of peristaltic motion, that is a formation of an inside movable circulating bolus that is closed by numerous streamlines, and shifts with the peristaltic wave at the speediness of waves. This phenomenon is useful in grasping the motion of the gastrointestinal tract and in the arrangement of thrombus in veins. Figures-(22-25) show various values of effective parameters on the trapping stream lines. The influence of the viscosity parameter (α) on trapping is analyzed in Figure-22 which depicts that the magnitude of the trapped bolus increases with an increased values of (α). This observation reveals a very significant phenomenon that, as the fluid viscosity is reduced, the bolus size is increased. The effect of Hartman number is calculated through Figure-23. It is observed that the larger size of the bolus becomes smaller with the increase of Hartman number. This result is expected since the Lorentz force opposes the fluid flow and, hence, decreases the fluid velocity. Therefore, we make here a significant notice that bolus formation can be averted by setting the force of the applied magnetic field. Figures-(24-25) exhibit that the volume of the bolus raises with increasing of the Grashof number and the heat source / sink parameter .

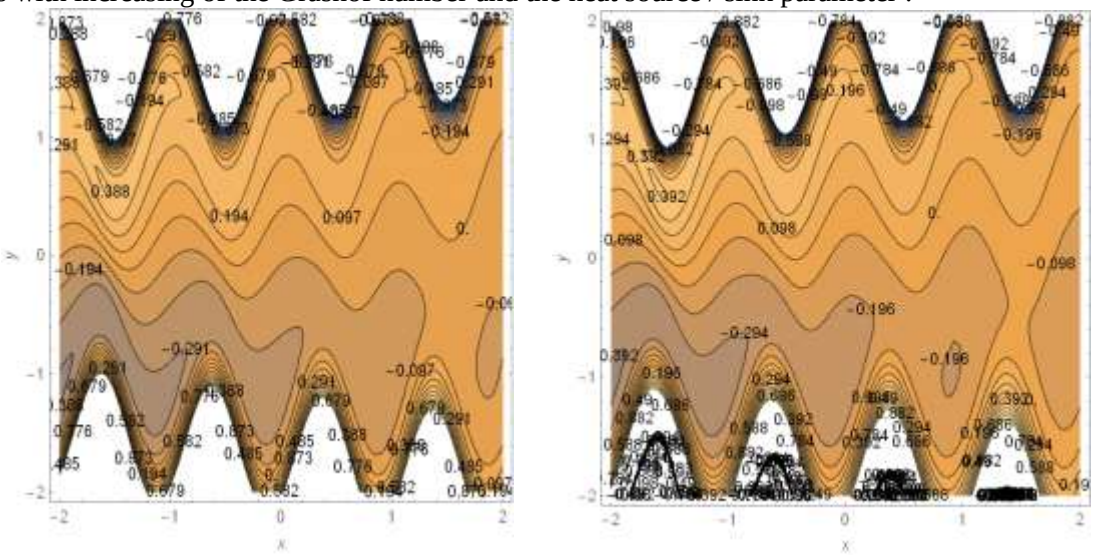

(a) (b)

**Figure 22**-The effect of (α) on the streamlines at $= 0.5, b = 0.5, \varphi = \mathrm{Pi}/4, t = 0.3, m = 0.1, Q = 2.4, \beta_1 = 0.5, \zeta = \mathrm{Pi}/4, k = 1.5, \mathrm{Gr} = 2, \mathrm{Nr} = 0.8, \beta = 1, M = 4, d = 1$ , $Sc = 2, \mathrm{Sr} = 3,\ \mathrm{Gm} = 2$ . (a) α =0.1 (b) α =0.5.

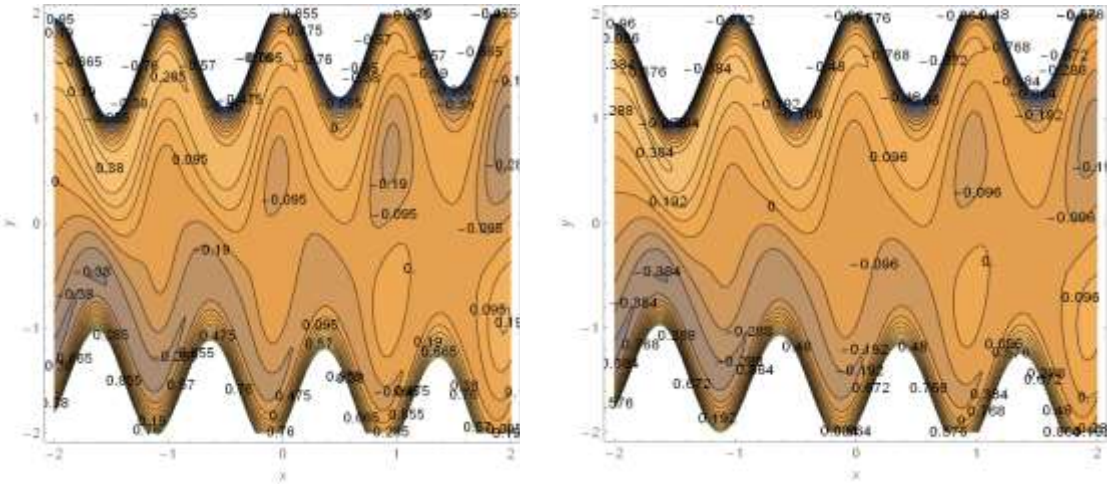

(a) (b)

**Figure 23**-The effect of (M) on the streamlines at $= 0.5, b = 0.5, \varphi = \mathrm{Pi}/4, t = 0.3, m = 0.1, Q = 2.4, \beta_1 = 0.5, \zeta = \mathrm{Pi}/4, k = 1.5, \alpha = 0.05, \mathrm{Nr} = 0.8, \beta = 1, Gr = 2, d = 1$ , $\mathrm{Sc} = 2, \mathrm{Sr} = 3,$ $\mathrm{Gm} = 2$ . (a) M=3 (b)M=4.

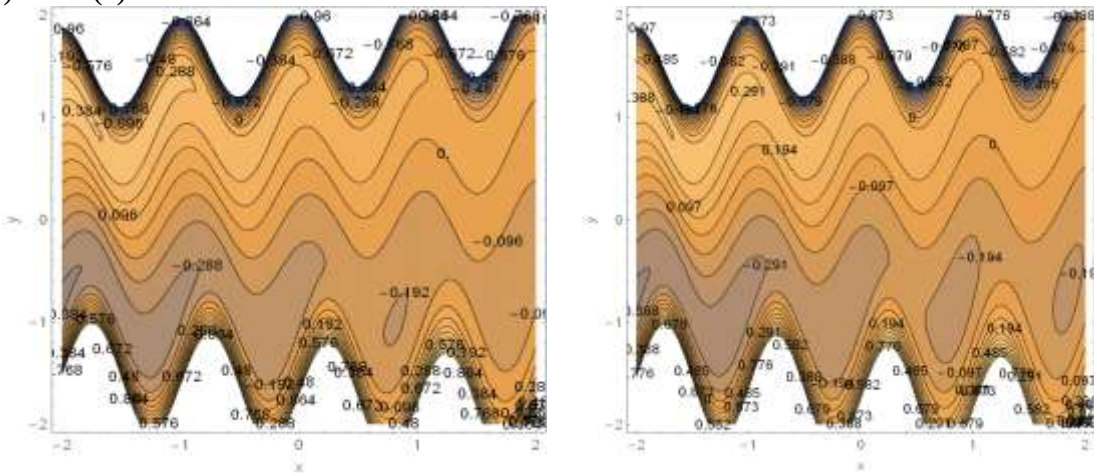

(a) (b)

**Figure 24**-The effect of (Gr) on the streamlines at $= 0.5, b = 0.5, \varphi = \mathrm{Pi}/4, t = 0.3, m = 0.1, Q = 2.4, \beta_1 = 0.5, \zeta = \mathrm{Pi}/4, k = 1.5, \alpha = 0.05, \mathrm{Nr} = 0.8, \beta = 1, M = 4, d = 1$ , $\mathrm{Sc} = 2, \mathrm{Sr} = 3,$ $\mathrm{Gm} = 2$ . (a) Gr=5 (b) Gr=8.

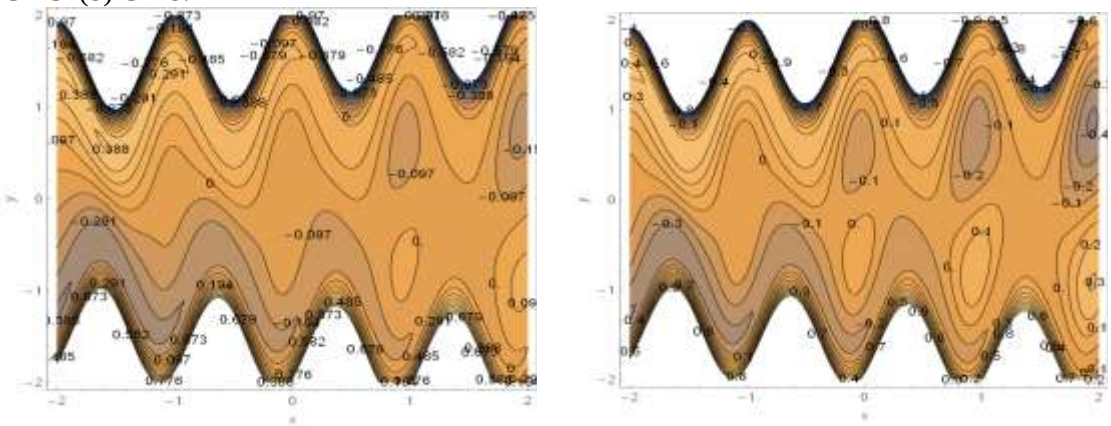

(a) (b)

**Figure 25**-The effect of ($\beta$) on the streamlines at $= 0.5, b = 0.5, \varphi = \mathrm{Pi}/4, t = 0.3, m = 0.1, Q = 2.4, \beta_1 = 0.5, \zeta = \mathrm{Pi}/4, k = 1.5, \alpha = 0.05, \mathrm{Nr} = 0.8, Gr = 2, M = 4, d = 1$ , $\mathrm{Sc} = 2, \mathrm{Sr} = 3,$ $\mathrm{Gm} = 2$ . (a)$\beta$=5 (b)$\beta$=8.

**9- Conclusions**

In this paper, we studied the peristaltic flow of variable viscosity fluid in porous medium through the tapered inclined asymmetric channel, under the impact of magnetic field, heat, and mass transfer . The channel asymmetry was generated by selecting the peristaltic waves on the non-uniform walls to have various amplitudes and phases. The solution was acquired by taking assumptions of lengthy wavelength approximation and small Renolds number. The main results and conclusions of this investigation are summarized as follows.

- The slip and no-slip conditions do not influence the fluid velocity with the increase of the values of (Gm) and (m).
- The (Gr) and (M) parameters have different effects on velocity for both models.
- The increase of the mean flow rate (Q) leads to an increase in the velocity in model-1 and a decrease near the walls in model -2.
- The temperature distribution is a decreasing function with rising values of (Nr) and an increasing function with the enhancement of the values of (β), ($\varphi$), ($b$) and (a).
- The concentration profile is diminished due to an increase in (Sr), (Sc), (β), (m), whereas it increases with the parameter (φ) and (Nr).
- Pressure gradient decreases with the increase of the inclination angle, Grashof number and volume flow rate, while this trend is reversed in the couple stress parameter.
- Increasing of the megnetic filed decreases the peristaltic pumping size of the trapped bolus.
- The magnitude of the trapped bolus increases through the increase of Grashof number , the heat source/sink parameter, and viscosity.

**References**


**1.** Rabby, M.G., Razzak ,A. and Molla,M.M. **2013**. Pulsatile non-Newtonian blood flow through a model of arterial stenosis. *Procedia Engineering*. **56**(5): 225-231.

**2.** Falk, E., Prediman, K.S. and Fuster, V. **1995**. Coronary plaque disruption Circulation. **92**(3): 657-671.

**3.** Burns, J. C. and Parkes **1967**.T. Peristaltic motion. *Journal of Fluid Mechanics*, **29**: 731-743.

**4.** Jaffrin, M. Y., Shapiro, A. H. and Weinberg, S. L. **1969**. Peristaltic pumping with long wavelength at low Reynolds numbers, *Journal of Fluid Mechanics*, **37**: 799–825.

**5.** Lew, H. S., Fung Y. C. and Lowenstein, C. B. **1971**. Peristaltic carrying and mixing of chyme in the small intestine, *Journal of Biomechanics*, **4**: 297–315.

**6.** Elshehawey, E.F. and Gharsseldien, Z.M. **2004**. Peristaltic transport of three-layered flow with variable viscosity. *Appl. Math. Computation*, **153**: 417–432.

**7.** Abd El Naby, A., El Misery, A.E.M. and El Shamy I.I. **2004**. Effects of an endoscope and fluid with variable viscosity on peristaltic motion, *Applied Mathematics and Computation*, **58**( 2) : 497-511.

**8.** Hayat, T.and Ali, N. **2008**. Effect of Variable Viscosity on the Peristatic Transport of a Newtonian Fluid in an Symmetric Channel. *Appl. Math. Modell*. **32**: 761-774.

**9.** Nadeem S., Hayat T., Akbar N.S. and Malik M.Y. **2009**. On the influence of heat transfer in peristalsis with variable viscosity. *Int. J. Heat Mass Transfer*. **52**: 4722-4730.

**10.** Farooq, S., Awais, M., Naseem, M., Hayat, T. and Ahmad, B. **2017**. Magnetohydrodynamic peristalsis of variable viscosity Jeffrey liquid with heat and mass transfer, *Nuclear Engineering and Technology*, **49**: 1396-1404.

**11.** Tripathi, B. and Sharma, B.K. **2018**. Effect of Variable Viscosity on MHD Inclined Arterial Blood Flow with Chemical Reaction. *Int. J. of Applied Mechanics and Engineering*, **23**(3): 767-785.

**12.** Huda, A. B., Akbar, N. Sh., Beg, O. A., Khan and M. Y. **2017**. Dynamics of variable-viscosity nanofluid flow with heat transfer in a flexible vertical tube under propagating waves. *Results in Physics*, **7**: 413–425.

**13.** Zin, N.A.M., Khan, I. and Shafie, S. **2016**. The impact silver nanoparticles on MHD free convection flow of Jeffrey fluid over an oscillating vertical plate embedded in a porous medium. *J. Mol. Liq*. **222**: 138–150.

**14.** Gul, A., Khan, I. and Shafie, S. **2015**. Energy transfer in mixed convection MHD flow of nanofluid containing different shapes of nanoparticles in a channel filled with saturated porous medium. *Nanoscale Res. Lett*. **10**: 490.
**15.** Abdellateef, A. I. and Zahoor ul Haque, S. **2016**. Peristaltic Flow of Newtonian Nanofluid through an Inclined Annulus Cylinder. *European Journal of Pure and Applied Mathematics*, **9**(3) : 266-276.
**16.** Kothandapani, M., Prakash, J. and Pushparaj, v. **2015**. Analysis of Heat and Mass Transfer on MHD Peristaltic Flow through a Tapered Asymmetric Channel. *Journal of Fluids*. (2015): Article ID 561263.
**17.** Ramesh, K. and Devakar, M. **2015**. Effects of Heat and Mass Transfer on the Peristaltic Transport of MHD Couple Stress Fluid through Porous Medium in a Vertical Asymmetric Channel, *Journal of Fluids* Article ID 163832:19.
**18.** Alharbi, M.S., Bazid, A. A.M. and El Gendy3,S.M. **2010**. Heat and Mass transfer in MHD Visco-Elastic Fluid Flow through a Porous Medium over a Stretching Sheet with Chemical Reaction. *Applied Mathematics*, **1**: 446-455
**19.** Reddy, M. G. **2016**. Heat and mass transfer on magnetohydrodynamic peristaltic flow in a porous medium with partial slip. *Alexandria Engineering Journal*, **55**: 1225–1234.
**20.** Misra, J.C., Mallick, B. and Sinha A. **2018**. Heat and mass transfer in asymmetric channels during peristaltic transport of an MHD fluid having temperature-dependent properties. *Alexandria Engineering Journal*, **57**: 391–406.
**21.** Slattery, J.C. **1972**. *Momentum Energy and Mass Transfer in Continua*. McGraw Hill, New York.